Journal of
Applied Crystallography
ISSN 0021-8898

Received 20 December 2007
Accepted 6 August 2008

Thermoelastic properties of magnesiowüstite, $(Mg_{1-x}Fe_x)O$: determination of the Anderson–Grüneisen parameter by time-of-flight neutron powder diffraction at simultaneous high pressures and temperatures

Ian G. Wood,[a]* Lidunka Vočadlo,[a] David P. Dobson,[a,b] G. David Price,[a] A. D. Fortes,[a] Frances J. Cooper,[c,a] J. W. Neale,[a] Andrew M. Walker,[a,d] W. G. Marshall,[e] M. G. Tucker,[e,d] D. J. Francis,[e] H. J. Stone[f,d,g] and C. A. McCammon[b]

[a]Department of Earth Sciences, University College London, Gower Street, London WC1E 6BT, UK, [b]Bayerisches Geoinstut, Universität Bayreuth, D-95440 Bayreuth, Germany, [c]Department of Earth Sciences, University of Southern California, 3651 Trousdale Parkway, Los Angeles, California 90089, USA, [d]Department of Earth Sciences, University of Cambridge, Downing Street, Cambridge CB2 3EQ, UK, [e]ISIS Facility, STFC Rutherford Appleton Laboratory, Harwell Science and Innovation Campus, Chilton, Didcot, Oxon OX11 0QX, UK, [f]Department of Materials Science and Metallurgy, University of Cambridge, Pembroke Street, Cambridge CB2 3QZ, UK, and [g]Materials Science Centre, University of Manchester, Grosvenor Street, Manchester M1 7HS, UK. Correspondence e-mail: ian.wood@ucl.ac.uk

The ability to perform neutron diffraction studies at simultaneous high pressures and high temperatures is a relatively recent development. The suitability of this technique for determining P–V–T equations of state has been investigated by measuring the lattice parameters of $Mg_{1-x}Fe_xO$ (x = 0.2, 0.3, 0.4), in the range $P < 10.3$ GPa and $300 < T < 986$ K, by time-of-flight neutron powder diffraction. Pressures were determined using metallic Fe as a marker and temperatures were measured by neutron absorption resonance radiography. Within the resolution of the experiment, no evidence was found for any change in the temperature derivative of the isothermal incompressibility, $\partial K_T/\partial T$, with composition. By assuming that the equation-of-state parameters either varied linearly or were invariant with composition, the 60 measured state points were fitted simultaneously to a P–V–T–x equation of state, leading to values of $\partial K_T/\partial T = -0.024$ (9) GPa K^{-1} and of the isothermal Anderson–Grüneisen parameter $\delta_T = 4.0$ (16) at 300 K. Two designs of simultaneous high-P/T cell were employed during this study. It appears that, by virtue of its extended pressure range, a design using toroidal gaskets is more suitable for equation-of-state studies than is the system described by Le Godec, Dove, Francis, Kohn, Marshall, Pawley, Price, Redfern, Rhodes, Ross, Schofield, Schooneveld, Syfosse, Tucker & Welch [*Mineral. Mag.* (2001), **65**, 737–748].

1. Introduction

Magnesiowüstite (sometimes termed ferropericlase), $(Mg_{1-x}Fe_x)O$, and magnesium silicate perovskite, $MgSiO_3$, are thought to be the dominant components of the lower mantle of the Earth (Ringwood, 1962); geochemical arguments require a bulk composition approximating to $(Mg,Fe)_2SiO_4$ and high-pressure experiments reveal these two materials to be the stable phases at pressures in excess of about 24 GPa (corresponding to the seismic discontinuity at 670 km depth). Indeed, until very recently it was thought that these materials persisted to the Earth's outer core, but it has now been proposed that $MgSiO_3$ perovskite transforms into the so-called 'post-perovskite phase' with the $CaIrO_3$ structure (Murakami *et al.*, 2004; Oganov & Ono, 2004) at the D'' layer, which lies about 150 km above the core–mantle boundary at a pressure of approximately 127 GPa. If we wish to quantify the compositional, thermal and dynamic structure of the lower mantle in detail we have to be able to interpret seismic tomographic data, which in turn requires us to determine the density and the elastic properties of the mantle-forming materials as a function of composition, pressure and temperature (*e.g.* Bina & Helffrich, 1992; Mattern *et al.*, 2005; Trampert *et al.*, 2004; Deschamps *et al.*, 2005; Samuel *et al.*, 2005); mere knowledge of the expected crystal chemistry of the lower mantle is not sufficient.

In order to obtain thermoelastic properties such as density, ρ, incompressibility (bulk modulus), K, and thermal expansion coefficient, α, at extremes of pressure and temperature, two approaches may be used: computer simulation or experiment. With regard to the former, quantum mechanical calculations at 0 K are now routine and are producing increasingly reliable results as both methodology and computing power improve. Although, in principle, it is straightforward to extend this work to elevated temperatures, in practice it remains a non-trivial matter, requiring large amounts of computer time on the present generation of supercomputers (see *e.g.* Vočadlo *et al.*, 2003; Gillan *et al.*, 2006; Vočadlo, 2007).

Experimental determination of thermoelastic properties at lower-mantle conditions is similarly not trivial, since it is extremely difficult to achieve stably the requisite conditions of high pressure (up to 130 GPa) and temperature (up to 3000 K) simultaneously. Until very recently, such experiments have often produced results that were difficult to interpret unambiguously (*e.g.* Shim *et al.*, 2001), but advances in the combination of synchrotron X-ray sources with laser-heated diamond-anvil cells have now, for example, enabled diffraction patterns from $MgSiO_3$ to be obtained at simultaneous pressures and temperatures approaching 145 GPa and 2700 K (Guignot *et al.*, 2007; Shim *et al.*, 2008).

As an alternative to determining directly the values of K and α at extremes of pressure, P, and temperature, T, we can instead attempt to extrapolate data obtained at more modest conditions. However, this approach is also not without its problems, as it is then necessary to measure not only K and α, but also at least one of their first derivatives with respect to temperature and pressure, respectively. The derivatives of the isothermal incompressibility, K_T, and the isobaric volume coefficient of thermal expansion, α_P, are linked *via* the relationship

$$(\partial\alpha_P/\partial P)_T = K_T^{-2}(\partial K_T/\partial T)_P \qquad (1)$$

(see *e.g.* Bina & Helffrich, 1992), and thus only one derivative need be measured. The temperature dependence of K_T is commonly expressed in terms of the isothermal Anderson–Grüneisen parameter, δ_T; this dimensionless quantity may be written in a number of ways, possibly the most useful in the present context being

$$\delta_T = -(\partial \ln K_T/\partial \ln V) = -(1/\alpha_P K_T)(\partial K_T/\partial_T) \qquad (2)$$

or

$$\delta_T = -(\partial \ln \alpha_P/\partial \ln V) = -(K_T/\alpha_P)(\partial\alpha/\partial P), \qquad (3)$$

where V is the volume (see *e.g.* Bina & Helffrich, 1992; Poirier, 2000). Knowledge of the first derivatives of K and α through δ is, therefore, an essential minimum requirement if we wish to extrapolate accurately data obtained at modest P and T to the conditions that obtain in the lower mantle. A major disadvantage of this method, however, is the implicit assumption that the extrapolation to higher P and T does not cross a phase boundary; even subtle phase transformations will restrict the range over which a safe extrapolation can be made. In the present case of (Mg,Fe)O, a number of recent experiments have indicated that high-pressure transformations may occur: Kantor *et al.* (2006) have reported a transition in $Mg_{0.8}Fe_{0.2}O$ at 35 (1) GPa to a rhombohedrally distorted phase; Badro *et al.* (2003) and Lin *et al.* (2005) have shown that a change in the spin state of iron – without a change in crystal structure – produces a change in the physical properties of $Mg_{0.83}Fe_{0.17}O$ at a pressure of about 60 GPa (equivalent to a depth of about 2000 km); more recently, shock experiments have suggested that $(Mg_{0.6}Fe_{0.4})O$ transforms from the cubic sodium chloride structure to the hexagonal NiAs structure at around 120 GPa (Zhang & Gong, 2006).

Measurements of the elastic deformation of crystals under conditions of simultaneous high P and high T are very commonly carried out by means of X-ray diffraction. Over the past 20 years or so, the methodology for single-crystal X-ray diffraction studies using diamond-anvil cells has advanced considerably (see *e.g.* Angel *et al.*, 1992; Miletich *et al.*, 2000; Angel, 2000), and elegant experiments under conditions of hydrostatic pressure to 10 GPa are now readily performed at room temperature. Similar studies at simultaneous high P and high T are far less common, with the majority of such data being collected from powders (see *e.g.* Fei & Wang, 2000). Although angle-dispersive X-ray powder diffraction patterns have been collected recently under very extreme conditions, up to 140 GPa and 2700 K, by combining laser-heated diamond-anvil cells with synchrotron radiation (*e.g.* Guignot *et al.*, 2007; Shim *et al.*, 2008), energy-dispersive X-ray powder diffraction with a solid-state detector is commonly employed; pressures are generated either in a multi-anvil press or by an externally heated diamond-anvil cell. The former enables very high temperatures to be attained at relatively modest pressures, whereas the latter is probably limited to about 1200 K in temperature but can achieve much higher pressures ($\sim$100 GPa). However, although data can be collected rapidly from very small samples, the powder diffraction patterns obtained from such energy-dispersive experiments often have rather low resolution [intrinsic to the solid state detector and small 2θ angle generally employed; *e.g.* those reported by Dong *et al.* (2003) have $\Delta d/d \simeq 1.7 \times 10^{-2}$] and sometimes display a high degree of line broadening (*e.g.* Duffy *et al.*, 1995; Scott *et al.*, 2001).

Although the pressures obtainable in neutron diffraction experiments are, as yet, relatively modest (Bailey, 2003), time-of-flight neutron powder diffraction would seem to offer some potential advantages over energy-dispersive X-ray methods (apart from the obvious greater sensitivity of neutrons to light atoms and magnetic structures, and their ability to determine bulk, rather than surface, properties of materials that absorb X-rays strongly – none of which are relevant in the present case). In particular, since the resolution in a time-of-flight pattern is effectively independent of d spacing, accurate cell parameters may be obtained rapidly from strong, low-index Bragg reflections; in addition, data are also frequently obtainable simultaneously over a wide d-spacing range, to short d spacings (*e.g.* $4.0 > d > 0.4$ Å for the high-pressure facility at ISIS, see below), allowing accurate structure refinements to be made. For elastically soft materials for which

Table 1
Previous computational and experimental studies of $Mg_{1-x}Fe_x0$.

For details of the methods used to determine these values see text.

	$\partial K_T/\partial T$ (GPa K^{-1})	δ_T
Computational studies of MgO (x = 0)		
Matsui (1989)	−0.0506 (5)	–
Reynard & Price (1990)	–	6.3–5.9 (300 K); 5.9–4.6 (2000 K)
Isaak (1990)	–	5.4–4.4 (300 K); 4.5–2.8 (2000 K)
Inbar & Cohen (1995)	–	4.8 (300 K)
Matsui *et al.* (2000)	−0.028	–
Experimental studies of MgO (x = 0)		
Sumino *et al.* (1983)	−0.030	12.66 (100 K); 4.99 (1300 K)
Chopelas (1990)	–	6.5(5) (298 K)
Isaak *et al.* (1989)	−0.027 >< −0.032	5.1 (3) (300–1800 K)
Fei (1999)	−0.030 (3)	–
Dewaele *et al.* (2000)	−0.022 (3)	–
Aizawa & Yoneda (2006)	−0.025	–
Experimental studies of $Mg_{1-x}Fe_xO$		
Fei *et al.* (1992) (x = 0.4)	−0.027 (3)	4.3 (5)
Zhang & Kostak (2002) (x = 0.4)	−0.029 (3)	5.3 (6)
van Westrenen *et al.* (2005) (x = 0.36)	−0.020 (1)	3.3 (1)
Aizawa & Yoneda (2006) (x = 0.4)	−0.022	–

large volumes of sample are available (*e.g.* epsomite, $MgSO_4{\cdot}7H_2O$; Fortes *et al.*, 2006), very accurate thermoelastic properties may be obtained in the pressure range up to 0.55 GPa by combining high-pressure gas cells with instruments such as the high-resolution powder diffractometer (HRPD) at the ISIS neutron source, STFC Rutherford Appleton Laboratory, UK. For stiffer materials, such as those considered in the present paper, much higher pressures are required and the problems are more challenging. Recent advances in neutron diffraction at simultaneous high P/T have been made at LANSCE (Los Alamos National Laboratory, USA) by Zhao *et al.* (1999) and also at ISIS, where a high-P cell with internal heating of the sample has been developed (LeGodec *et al.*, 2001) for the PEARL beamline high-pressure facility, HiPr, a medium-resolution high-flux diffractometer dedicated to high-pressure studies. A novel feature of the latter apparatus is that it permits the *in situ* measurement of the sample temperature by neutron absorption resonance radiography (Stone *et al.*, 2005, 2006).

The purpose of the present experiment was, therefore, twofold. Firstly, we wished to undertake a pilot study using the new high-P/T cell at ISIS to assess the accuracy and speed with which thermoelastic properties might be determined; $(Mg_{1-x}Fe_x)O$ provided an ideal test material for this purpose as its high-symmetry face-centred cubic structure and small unit cell allowed short data collection times. Secondly, because of its importance in the lower mantle, we wished to add to the relatively sparse experimental data that were then available for this material, Hama & Suito (1999) in their paper on thermodynamic modelling of magnesiowüstite having pointed out that 'As for magnesiowüstite, due to the fewness of the experimental data for various iron-concentrations under high pressure and high temperature, the examination of our model was rather limited.'

2. Previous computational and experimental studies of the thermoelastic properties of $(Mg_{1-x}Fe_x)O$

For convenience, the available values of $\partial K_T/\partial T$ and/or of δ_T from previous computational and experimental studies are listed in Table 1; brief details of the methods employed in these various studies are given below.

A number of computer simulations of the properties of the end member, MgO, have been published, leading to values either of $\partial K_T/\partial T$ or of δ_T. By fitting the values of K_T derived by Matsui (1989), using molecular dynamics with pair potentials and quantum corrections over the range 300–1500 K, a value of $\partial K_T/\partial T = -0.0506$ (5) GPa K^{-1} is obtained. Reynard & Price (1990), using many-body atomistic potentials, found that, for the pressure range 5–120 GPa, δ_T varied from 6.3 to 5.9 at 300 K and from 5.9 to 4.6 at 2000 K; they therefore concluded that δ_T could be assumed constant to the core–mantle boundary. Isaak (1990) employed a potential-induced breathing (PIB) model (an *ab initio* method) and found that at 300 K δ_T varied with compression from 5.4 (for P = 0 and $V = V/V_o$) to 4.4 (for $\eta = V/V_o = 0.7$), whereas at 2000 K, δ_T varied from 4.5 (P = 0) to 2.8 (η = 0.7). Inbar & Cohen (1995), using a variational induced breathing (VIB) model based on density functional theory, found δ_T = 4.8 (at ambient conditions); they also examined the suggestion by Anderson & Isaak (1993) that $\delta_T = \delta_{To}\eta^{\kappa}$ (where κ = 1.4), concluding that this approximation held only to η = 0.8. Matsui *et al.* (2000), using molecular dynamics, *via* a breathing shell model with quantum corrections, reported that their results for K_T at P = 0 agreed very well with the experiments of Isaak *et al.* (1989) over the temperature range 300–1800 K and gave a value for $\partial K_T/\partial T = -0.028$ at 300 K. Their plot of K_T *versus* T appears to have a very slightly shallower slope than that of Isaak *et al.* (1989) in the range 300–600 K; in the range 1500–1800 K the results of Matsui *et al.* (2000) appear effectively identical to those of Isaak *et al.* (1989), with the magnitude of $\partial K_T/\partial T$ becoming slightly greater at increased T ($\simeq -0.03$ GPa K^{-1}).

Experimental determinations of $\partial K_T/\partial T$ for MgO have been reported by Sumino *et al.* (1983), who found $\partial K_T/\partial T = -0.030$ GPa K^{-1} by ultrasonic measurements over the range $80 < T < 1800$ K, with δ_T varying from 12.66 at 100 K to 4.99 at 1300 K. Chopelas (1990), using an indirect method, primarily from heat capacity measurements, found δ_T = 6.5 (5) at 298 K. Isaak *et al.* (1989) determined the elastic moduli of single-crystal MgO to 1800 K by ultrasonic resonance, giving values of $\partial K_T/\partial T$ in the range from −0.027 to −0.032 GPa K^{-1}. Fei (1999) employed an externally heated diamond-anvil cell with energy dispersive powder diffraction and synchrotron radiation to obtain $\partial K_T/\partial T = -0.030$ (3) GPa K^{-1}, whereas Dewaele *et al.* (2000), using monochromated synchrotron radiation, found $\partial K_T/\partial T = -0.022$ (3) GPa K^{-1}. By fitting P–V–T equations of state to the data for MgO collected by

Utsumi *et al.* (1998), Dewaele *et al.* (2000) and Speziale *et al.* (2001), Aizawa & Yoneda (2006) obtained a value of $\partial K_T/\partial T = -0.025$ GPa K^{-1}; a similar procedure (see below) was also applied by these authors to data sets from $Mg_{0.6}Fe_{0.4}O$.

The properties of (Mg,Fe)O at room temperature have been examined by a number of workers. For $Mg_{0.6}Fe_{0.4}O$, compression data at room temperature to 26.4 GPa using a diamond-anvil cell have been reported by Rosenhauer *et al.* (1976). Richet *et al.* (1989) made similar measurements at ambient temperature with a diamond-anvil cell to 50 GPa, for both $Mg_{0.6}Fe_{0.4}O$ and $Mg_{0.8}Fe_{0.2}O$; angle-dispersive X-ray powder diffraction patterns taken with Mo $K\alpha$ radiation were recorded photographically. A single-crystal X-ray diffraction study of $Mg_{0.63}Fe_{0.27}O$ covering a similar pressure range, to 51 GPa, has been made by Jacobsen *et al.* (2005). Following an earlier study by Reichmann *et al.* (2000) using ultrasonics, Jacobsen, Reichmann *et al.* (2002) carried out an extremely thorough investigation of the elastic properties of $Mg_{1-x}Fe_xO$ across a wide range of compositions at room temperature by means of ultrasonic interferometry and single-crystal X-ray diffraction. In addition, the variation with pressure of the elastic constant c_{11} for MgO and $Mg_{0.423}Fe_{0.541}O$ has been determined using high-pressure ultrasonics by Jacobsen, Spetzler *et al.* (2002). A further recent ultrasonic study of $Mg_{1-x}Fe_xO$ at high pressure (Jacobsen *et al.*, 2004) has indicated an unexpected behaviour in c_{44}, with pressure-induced softening observed for compositions with $x > 0.5$. Brillouin scattering has also been used to measure the elastic properties of $Mg_{0.94}Fe_{0.06}O$ (Jackson *et al.*, 2006).

At high temperatures, Fei *et al.* (1992) examined $Mg_{0.6}Fe_{0.4}O$ using an externally heated diamond-anvil cell at simultaneous high P and T. Here, X-ray powder data were collected by energy dispersive diffraction with synchrotron radiation over the range $P < 30$ GPa and $300 < T < 800$ K, leading to values of $\partial K_T/\partial T = -0.027$ (3) GPa K^{-1} and $\delta_T = 4.3$ (5) above the Debye temperature, which was estimated to be 500 (2) K. The alternative approach of using a multi-anvil press has been taken by Zhang & Kostak (2002), who studied $Mg_{0.6}Fe_{0.4}O$ to 10.1 GPa over the range 300–1273 K and found $\partial K_T/\partial T = -0.029$ (3) GPa K^{-1}. Recently, during the course of the present work, van Westrenen *et al.* (2005) reported a study of $Mg_{0.64}Fe_{0.36}O$, by means of energy-dispersive synchrotron X-ray powder diffraction in a multi-anvil press; they measured 53 data points in the range up to $P = 26.7$ GPa and $T = 2173$ K, using gold and MgO as pressure markers. By combining their data with those of Fei *et al.* (1992) and Zhang & Kostak (2002), a total of 165 P–V–T measurements were then fitted to a high-T third-order Birch–Murnaghan equation of state [using the program *EOSFIT* (Angel, 2000)], leading to values of $\partial K_T/\partial T = -0.020$ (1) GPa K^{-1} and $\delta_T = 3.3$ (1). Although the precision with which $\partial K_T/\partial T$ has been determined is very good, its value seems somewhat lower than might be expected from the results of both Fei *et al.* (1992) and Zhang & Kostak (2002); this might possibly reflect the fact that a single V_o parameter was assumed for the combined data set and thus the possibility of systematic offsets in the lattice parameters from the three experiments was neglected. Nevertheless, the results of van Westrenen *et al.* (2005) provide an excellent benchmark against which to assess the present study, as they represent the combined work of three research groups over a number of years. Even more recently, a re-examination of these three data sets has been reported by Aizawa & Yoneda (2006), who derived a value of $\partial K_T/\partial T = -0.022$ GPa K^{-1}.

3. Experimental Details

Samples of composition $Mg_{1-x}Fe_xO$, with $x = 0.2$, 0.3 and 0.4, were prepared at the Bayerisches Geoinstut, Universität Bayreuth, Germany (BGI), by sintering the appropriate mixtures of MgO, Fe and Fe_2O_3 at 1573 K at an oxygen fugacity just below the Fe–'FeO' buffer. In order to extend the range of compositions studied, an end-member MgO sample was also measured, although these data were later discarded (see below); the MgO (BDH, AnalaR grade) was cold pressed into pellets and then sintered at 1373 K in air. During the neutron diffraction experiments the furnace and sample are not isolated from the atmosphere and it was, therefore, decided to use iron as a pressure marker so as to ensure that the samples remained in a reducing environment throughout the experiments. The three $Mg_{1-x}Fe_xO$ samples were each mixed with approximately 15 wt% of Fe, whereas for the MgO sample a piece of Fe foil 50 µm thick and 2.5 mm in diameter placed centrally in the sample was used. Since the samples would be in direct contact with the heating element in the pressure cell, it was important not to exceed the percolation threshold for electrical conduction, expected to be ~14% Fe by volume. Mössbauer spectra were measured, at the BGI, from all three $(Mg_{1-x}Fe_x)O$ samples before the neutron diffraction data were collected and from two of them ($x = 0.2$ and 0.4) afterwards; in no case was any Fe^{3+} detectable (the detection limit was 1% of the total Fe present in the phase), indicating that there had been no change from the starting composition during the high-P/T experiment.

The use of metallic iron as a pressure marker has a number of disadvantages. Firstly, the P–V–T equation of state of α-iron (see *e.g.* Zhang & Guyot, 1999*a*; Anderson & Isaak, 2000) is probably less well known than that of other materials such as NaCl. Secondly, α-iron undergoes a number of phase transitions and reactions. The high-temperature transition in α-iron from a ferromagnetic to a paramagnetic state produces an appreciable effect on the unit-cell volume (see *e.g.* Besson & Nicol, 1990); this transition occurs at 1073 K at ambient pressure, with the transition temperature showing little, if any, pressure dependence [Leger *et al.* (1972) give a value of 0.3 K GPa^{-1}]. Furthermore, at high temperatures α-iron transforms into fcc-structured γ-iron, and at high pressures to hcp-structured ε-iron (see *e.g.* Besson & Nicol, 1990; Zhang & Guyot, 1999*b*); it may also react with the graphite furnace of the high-P/T cell to form an iron carbide. In some cases these constraints set an upper limit to the usable range of temperature (see below).

The neutron powder diffraction patterns were collected by the time-of-flight method with the PEARL Beamline high-

Table 2
Refined values of the lattice parameters of $Mg_{1-x}Fe_xO$ and Fe.

Figures in parentheses are estimated standard uncertainties from the Rietveld refinements and refer to the least significant figures. The estimated uncertainties in the temperature measurements from the width of the Ta resonance are approximately ±15 K. The pressures were obtained from the equation of state of α-iron (for details see text). For each composition the measurements were made in the order in which they are listed.

(*a*) $Mg_{0.8}Fe_{0.2}O$.

$a(Mg_{0.8}Fe_{0.2}O)$ (Å)	a(Fe) (Å)	T (K)	P (GPa)
4.23395 (11)	2.86330 (26)	291	0.00 (6)
4.22346 (20)	2.85847 (37)	328	1.08 (8)
4.22435 (21)	2.85933 (36)	414	1.43 (8)
4.23002 (21)	2.86307 (39)	511	1.33 (8)
4.23511 (20)	2.86726 (35)	584	1.02 (7)
4.24004 (21)	2.87114 (37)	691	0.96 (7)
4.21480 (21)	2.85253 (37)	352	2.31 (8)
4.21659 (21)	2.85409 (36)	421	2.43 (8)
4.22149 (22)	2.85737 (40)	527	2.44 (8)
4.22583 (24)	2.86115 (40)	641	2.41 (8)
4.23184 (22)	2.86550 (38)	697	1.95 (8)
4.20872 (21)	2.84900 (35)	370	3.09 (8)
4.20990 (19)	2.84974 (31)	410	3.19 (7)
4.21432 (23)	2.85269 (36)	537	3.36 (8)
4.22435 (18)	2.85906 (32)	730	3.27 (7)
4.23745 (20)	2.86771 (37)	929	2.82 (7)
4.24840 (20)	2.87302 (80)†‡	1107	2.83 (13)
4.21038 (15)	2.84771 (35)	357	3.26 (8)
4.21559 (14)	2.85064 (31)	525	3.68 (7)
4.22164 (13)	2.85558 (32)	711	3.80 (7)
4.22826 (14)	2.86148 (36)	877	3.62 (7)
4.23735 (16)	2.86621 (70)†‡	1090	3.88 (12)
4.20460 (12)	2.84360 (32)	363	4.11 (8)
4.20898 (12)	2.84690 (32)	534	4.45 (8)
4.21485 (16)	2.85040 (44)	739	4.91 (9)
4.21384 (14)	2.84992 (37)	767	5.16 (8)
4.22044 (15)	2.85650 (39)	917	4.72 (8)
4.22914 (16)	2.85995 (99)†‡	1126	5.14 (16)
4.19971 (13)	2.84034 (34)	390	4.92 (8)
4.20413 (17)	2.84334 (46)	544	5.21 (10)
4.20979 (15)	2.84686 (40)	720	5.49 (9)
4.21606 (15)	2.85270 (41)	919	5.43 (8)
4.22436 (16)	2.85658 (96)†‡	1129	5.75 (16)
4.25464 (16)	2.87874 (37)	986	1.30 (7)
4.26321 (17)	2.88308 (58)†‡	1174	1.57 (9)
4.23706 (16)	2.86517 (37)	378	0.19 (8)

(*b*) $Mg_{0.7}Fe_{0.3}O$.

$a(Mg_{0.7}Fe_{0.3}O)$ (Å)	a(Fe) (Å)	T (K)	P (GPa)
4.25388 (15)	2.86743 (31)	298	0.00 (8)
4.23376 (23)	2.85674 (44)	298	1.93 (10)
4.22305 (28)	2.85000 (47)	298	3.22 (11)
4.21721 (27)	2.84505 (46)	298	4.20 (11)
4.19288 (29)	2.82810 (40)	298	7.81 (11)
4.17493 (29)	2.81731 (43)	298	10.32 (11)
4.18955 (24)	2.82746 (39)	621	9.82 (10)
4.21902 (17)	2.84742 (91)	719	6.14 (18)
4.21233 (15)	2.84102 (99)	523	6.34 (20)
4.21395 (15)	2.84074 (65)	496	6.25 (14)
4.22106 (15)	2.84780 (50)	735	6.15 (11)
4.22382 (22)	2.84772 (45)	542	5.10 (10)
4.22414 (21)	2.84719 (43)	518	5.07 (10)
4.23330 (19)	2.85518 (40)	726	4.68 (9)
4.22849 (19)	2.85147 (38)	518	4.23 (9)
4.23676 (19)	2.85810 (41)	748	4.25 (9)
4.24091 (19)	2.86080 (40)	548	2.65 (9)
4.25665 (17)	2.87050 (38)	763	2.12 (8)

(*c*) $Mg_{0.6}Fe_{0.4}O$.

$a(Mg_{0.6}Fe_{0.4}O)$ (Å)	a(Fe) (Å)	T (K)	P (GPa)
4.25691 (12)	2.86473 (22)	290	0.00 (5)
4.25665 (17)	2.86834 (26)	534	0.80 (6)
4.29171 (13)	2.88761 (33)	982	0.15 (6)
4.25430 (13)	2.86257 (24)	524	1.75 (6)
4.27757 (15)	2.87867 (33)	984	1.54 (6)
4.24745 (13)	2.85761 (24)	523	2.64 (6)
4.26876 (14)	2.87156 (33)	961	2.58 (6)
4.24089 (13)	2.85288 (25)	551	3.68 (6)
4.26075 (14)	2.86591 (34)†	983	3.65 (6)
4.23477 (13)	2.84938 (24)	549	4.34 (6)
4.25268 (15)	2.86076 (37)†	982	4.54 (7)

† Data showed reflections from both α-iron and γ-iron. ‡ Data not used in fitting the equations of state, as they lie above the Curie temperature of α-iron and hence the calculated pressure values may not be reliable.

pressure facility, HiPr (ISIS Annual Report, 1996), at the ISIS neutron source, STFC Rutherford Appleton Laboratory, UK. This medium-resolution, high-flux diffractometer is optimized for data collection from a Paris–Edinburgh press with opposed anvils. The $2\theta = 90^\circ$ scattering geometry was used, with the incident beam running along the axis of the Paris–Edinburgh load frame and the diffracted beams emerging in the gap between the tungsten carbide (WC) anvils. Nine detector modules constitute the main transverse detector bank, covering the scattering angle interval $83 < 2\theta < 97^\circ$, which typically yield diffraction patterns over the d-spacing range $\sim 0.5 < d < 4.1$ Å at a resolution of $\Delta d/d \simeq 0.8\%$. Diffraction data at each P/T point were collected usually for between 20 and 50 min, with longer times being required at higher pressures owing to the gradual closure of the gap between the anvils, which restricts the diffracted beams. In most cases, however, the limiting factor in data collection was not the time required for acquisition of the diffraction pattern but rather the time needed to measure the Ta neutron absorption resonance with sufficiently good counting statistics to allow a precise determination of the sample temperature (see below).

For our first experiments, on the $Mg_{0.8}Fe_{0.2}O$ and $Mg_{0.6}Fe_{0.4}O$ samples, the high-P/T apparatus developed by Le Godec *et al.* (2001) was used. Two 50 µm-thick Ta foils were placed at the centre of each sample to allow determination of the temperature from the width of the Ta absorption resonance, typically to a precision of ±15 K; full details of the procedure used are given by Stone *et al.* (2005, 2006). During these experiments, we attempted to collect the data (see Table 2) along a chosen set of isotherms and isobars. However, in this experimental arrangement the degree of gasket flow is such that it has not proved possible to incorporate a thermocouple into the high-pressure volume to provide an instantaneous measurement of the sample temperature; similarly, the sample pressure is not known accurately until the diffraction data are analysed. Thus, the best that can be achieved in respect of isothermal or isobaric conditions is to operate the apparatus at a chosen set of heater powers and of oil-pressures in the ram of the Paris–Edinburgh press. For $Mg_{0.8}Fe_{0.2}O$, 36 P–V–T points were measured in the range $P <$ 5.8 GPa and $300 < T < 1174$ K. For $Mg_{0.6}Fe_{0.4}O$, there was

sufficient time available to measure only 11 P–V–T points in the range $P < 4.5$ GPa and $300 < T < 984$ K.

A major beam failure at ISIS resulted in our experiment being carried out in two parts separated by a period of over 18 months. This gave us an opportunity to make an assessment of the capabilities of the high-P/T capsule and anvil assembly as designed by Le Godec *et al.* (2001) for equation-of-state studies; it was felt that the maximum pressure that we had been able to obtain in the experiments listed above (5.8 GPa) was rather too low to allow precise values of K_T to be determined. The Le Godec *et al.* (2001) design uses Bridgman-type anvils with conical cavities (Fig. 1*a*); the sample is contained within a cylindrical graphite heater held inside a pyrophyllite gasket that is in turn surrounded by a Teflon support ring. Although good diffraction data may be obtained in this way, the system suffers from the disadvantage that there is effectively no support for the gasket perpendicular to the axis of compression, which limits the maximum pressure attainable at the sample.

For the remaining experiments, using the MgO and $Mg_{0.7}Fe_{0.3}O$ samples, it was decided, therefore, to try a different form of high-P/T environment with toroidal gasket geometry, using an arrangement essentially similar to that proposed by Zhao *et al.* (1999) for neutron diffraction studies [see Fig. 1(*b*) for details]. There is a considerable literature on high-pressure apparatus using gaskets of this type, constructed typically from lithographic limestone (see *e.g.* Khvostantsev *et al.*, 1977, 1998, 2004). Here, the central, roughly spherical, part of the gasket containing the cylindrical sample is surrounded by an outer toroid of gasket material. This provides greater support, enabling, for example, pressures up to 12 GPa to be attained with a 15 mm-diameter high-pressure volume under a load of 380 tonnes (1 tonne load $\simeq 10^4$ N) (Khvostantsev *et al.*, 1998), which is well within the capabilities of a V7 Paris–Edinburgh load frame. The reduced gasket flow in this arrangement is advantageous in two respects: firstly, it reduces the amount of anvil closure, which in diffraction experiments reduces the strength of the diffracted beams; secondly, it reduces the likelihood of breakage of thermocouple leads (and other electrical connections to the high-pressure volume). For this initial, pilot experiment, which is the first high-P/T study that has been carried out at ISIS with the toroidal gasket system, we used a set of standard single-toroid 'Los Alamos profile' tungsten carbide anvils from ISIS, with a central 'sphere' of diameter ∼6 mm enclosing a cylindrical sample 3.2 mm in diameter and ∼2.5 mm long. The gasket used (Fig. 1*b*) was of a compound construction with an outer annulus machined from MgO enclosing an inner section fabricated from Y-stabilized ZrO_2. It was found that this setup enabled us to reach pressures roughly twice as great as those attainable with the design of Le Godec *et al.* (2001) whilst still giving good count rates. The system also appeared to be more thermally efficient, producing a roughly 50% greater temperature rise per watt of heater power (probably because of the good thermal insulation properties of the ZrO_2). The only disadvantage we encountered was that, partly owing to the lack of an incident-beam collimator of suitable diameter, the diffraction patterns were less clean, containing peaks from the components of the sample environment; work is currently in progress to eliminate these defects by better collimation.

The toroidally gasketted assembly used in the present study was found to have similar P/T performance to that previously described by Zhao *et al.* (1999). Our setup differs from theirs in three ways. Firstly, thin, tapered aluminium washers were placed on either side of the poly(tetrafluoroethene) (PTFE) support ring; these washers reduce the extrusion of the PTFE and hence allow it to give better support to the MgO gasket during the initial compression. Secondly, the toroidal gaskets were manufactured from MgO rather than zirconium phosphate (ZPM); although Zhao *et al.* (1999) report that ZPM is a better gasket material, we have found it to be less robust and more difficult to machine than MgO. Thirdly, the electrical connections between the WC anvils and the graphite furnace were made using thin Pt foil rather than coiled Pt wire, as we have found this to be a more reliable method.

Using the toroidal gasket system, 24 usable P–V–T points were collected from MgO in the range $P < 9.1$ GPa and $300 < T < 1011$ K (these data were later discarded; see §4 below). For

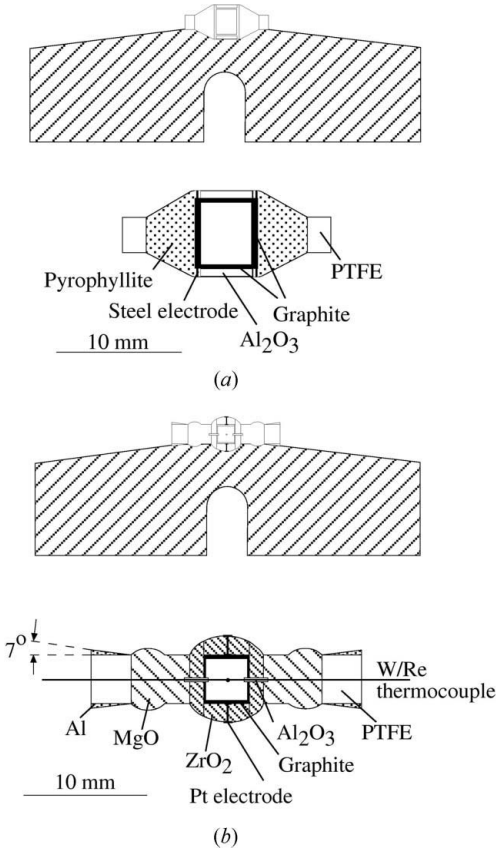

Figure 1
(*a*) The high-P/T sample/heater assembly used for the $(Mg_{0.8}Fe_{0.2})O$ and $(Mg_{0.6}Fe_{0.4})O$ samples [diagram after Le Godec *et al.* (2001)]. The upper diagram shows the assembly resting on one of the two tungsten carbide anvils; the lower diagram shows its detailed construction. (*b*). The toroidally gasketted, high-P/T sample/heater assembly used with the 'Los Alamos profile' anvils for the MgO and $(Mg_{0.7}Fe_{0.3})O$ samples. The upper diagram shows the assembly resting on one of the two tungsten carbide anvils; the lower diagram shows its detailed construction.

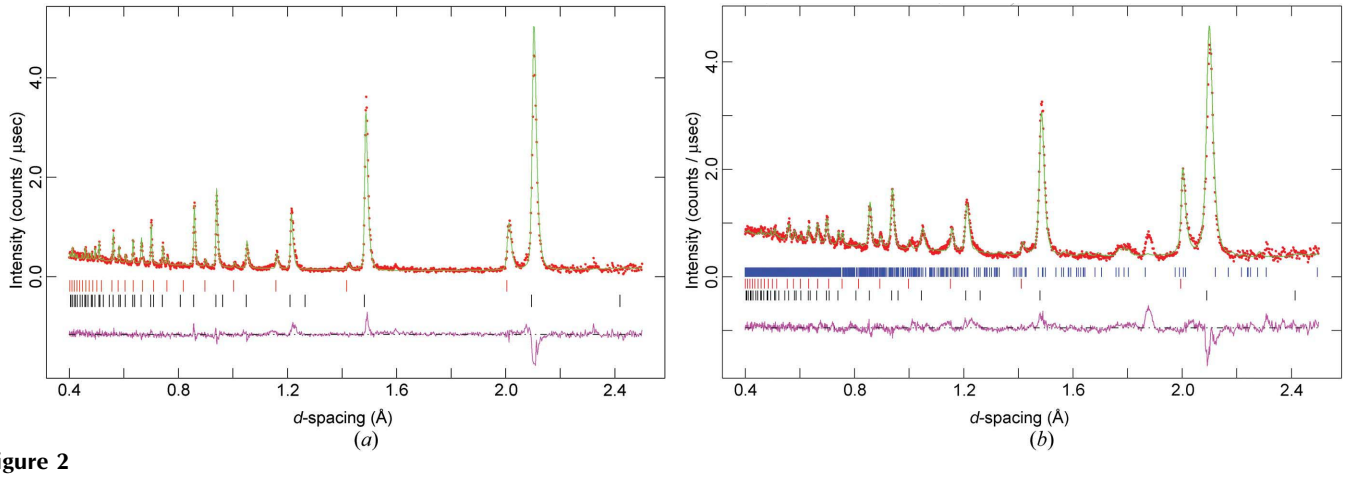

Figure 2
(*a*) Neutron powder diffraction pattern from $(Mg_{0.8}Fe_{0.2})O$ at 390 K and 4.92 GPa [data collected using the pressure cell as described by Le Godec *et al.* (2001); see Fig. 1(*a*)]. Observed data are shown as points, with the calculated pattern from the Rietveld refinement as a continuous line. The uppermost set of reflection markers are for Fe, the lower set for $(Mg_{0.8}Fe_{0.2})O$. The very weak peak at about 2.3 Å is from the Ta foil used to measure the sample temperature; the small feature between the reflections from Fe and $(Mg_{0.8}Fe_{0.2})O$ at about 2.05 Å is residual γ-iron/iron carbide (for details see text). (*b*) Neutron powder diffraction pattern from $(Mg_{0.7}Fe_{0.3})O$ at 621 K and 9.82 GPa [data collected using the pressure cell with toroidal gaskets; see Fig. 1(*b*)]. Symbols are as described for (*a*), but with an additional (uppermost) set of reflection markers for ZrO_2. The additional 'background', from the ZrO_2 gasket material, was seen at all pressures and temperatures and is especially noticeable for $1.5 < d < 2.0$ Å (note, however, that an incident beam collimator that was larger than optimal was used when collecting these data).

$Mg_{0.7}Fe_{0.3}O$, 18 P–V–T points in the range $P < 10.3$ GPa and $300 < T < 763$ K were measured (some data were collected from this sample to 1200 K but these were not usable because of transformation of the α-iron pressure marker). As before, Ta foil was placed at the centre of each sample (Hf foil was also included in the case of $Mg_{0.7}Fe_{0.3}O$) to allow determination of the temperature from the width of the absorption resonances.

In all cases the cell parameters were determined by Rietveld refinement using the program *GSAS* (Larson & Von Dreele, 2000) implemented *via EXPGUI* (Toby, 2001).[1] For the $Mg_{0.8}Fe_{0.2}O$ and $Mg_{0.6}Fe_{0.4}O$ samples, only the two major phases were included in the refinements, which converged with χ^2 typically between 1.5 and 2.0; although these data did show some very weak extra peaks in the diffraction patterns, which could be readily attributed to the alumina end caps of the gasket and to the Ta foil used to measure the temperature, it was found that including these phases in the refinement made a negligible difference to the lattice parameters of both Fe and $Mg_{1-x}Fe_xO$. Similarly, inclusion of the γ-iron phase, when this was present in noticeable amounts, changed the refined values of the lattice parameter of both Fe and $Mg_{1-x}Fe_xO$ by 0.2 s.u. at most, an amount judged to be negligible. The observed, calculated and difference patterns from one of the $Mg_{0.8}Fe_{0.2}O$ refinements (at 390 K, 4.92 GPa) are shown in Fig. 2(*a*).

The MgO and $Mg_{0.7}Fe_{0.3}O$ data, collected using the pressure cell employing the toroidal gaskets, showed much stronger reflections from components of the sample environment, principally from the ZrO_2 gasket (this was at least partly due to the fact that an incident-beam collimator of optimal size was not available and a larger one was used instead). X-ray powder diffraction of the ZrO_2 gasket material showed that it had the monoclinic baddeleyite structure (Smith & Newkirk, 1965). It was found that a significant improvement in the fit was obtained if this phase was included in the Rietveld refinement; only the lattice parameters and phase fraction of ZrO_2 were varied, the coordinates being fixed at the values given by Smith & Newkirk (1965). For these MgO and $Mg_{0.7}Fe_{0.3}O$ data, the refinements converged with χ^2 typically between 2 and 4; Fig. 2(*b*) shows the observed, calculated and difference patterns from $Mg_{0.7}Fe_{0.3}O$ at 621 K and 9.8 GPa.

4. Results and discussion

Table 2 lists the refined lattice parameters and sample temperatures for the data collected from the three $Mg_{1-x}Fe_xO$ samples; for each composition, the measurements were made in the order in which they are listed in the table. To convert the measured unit-cell volumes of Fe to the corresponding pressures, the parameters for the equation of state of α-Fe tabulated by Anderson & Isaak (2000) were assumed, with $K_{To} = 166.6$ GPa, $K'_o = \partial K_{To}/\partial P = 5.97$ (Rotter & Smith, 1966) (values taken to be at 300 K), and $\partial K_T/\partial T = -0.034$ GPa K^{-1}, $\alpha = 3.6 \times 10^{-5}$ K^{-1} (Isaak & Masuda, 1995). For each of the four materials examined, a data set had been collected very close to zero pressure and room temperature (T_{RT}); this was used to define $V_o(T_{RT})$ for Fe in each case. This volume was then adjusted to give the value of $V_o(T)$ at the measured temperatures of the other points, using the expression

$$V_o(T) = V_o(T_{RT}) \exp[\alpha(T - T_{RT})] \quad (4)$$

(Fei, 1995). Once $V_o(T)$ had been determined, the pressure was then calculated from a third-order Birch–Murnaghan equation of state,

[1] Supplementary data for this paper are available from the IUCr electronic archives (Reference: KS5172). Services for accessing these data are described at the back of the journal.

$$P = \frac{3K_{To}}{2}\left\{\left[\frac{V_o(T)}{V}\right]^{7/3} - \left[\frac{V_o(T)}{V}\right]^{5/3}\right\} \times \left(1 + \frac{3}{4}(K'_o - 4)\left\{\left[\frac{V_o(T)}{V}\right]^{2/3} - 1\right\}\right) \quad (5)$$

(see *e.g.* Poirier, 2000), using the appropriate temperature-corrected value of K_{To}. The resulting pressures are listed in Table 2. The uncertainty in the pressure was estimated from the slope of the Birch–Murnaghan P–V curve and the calculated uncertainty in (V_o/V); this is possibly an overestimate of the probable error, as the calculation assumes that the standard uncertainties in V_o and in V are independent of each other. Close attention was paid to data at pressures and temperatures where phase transformations of the α-iron might be expected. For several high-temperature data sets both α-iron and γ-iron were seen in the diffraction pattern; these are marked with the symbol '†' in Table 2 (a few data sets for which the transformation to γ-iron was complete had to be discarded and so are not listed). We found that some α-iron persisted to temperatures well above the α–γ phase boundary, which, as described for example by Zhang & Guyot (1999*b*), approximately follows the curve $T = 1183 - 88.5P + 3.9P^2$ (where T is measured in K and P in GPa). However, even if α-iron persists to high temperatures, it will becomes paramagnetic above its Curie temperature of 1073 K and its thermal expansion curve will change slope (see *e.g.* Besson & Nicol, 1990), as will its equation-of-state parameters. In principle, α-iron can still be used as a pressure marker above the Curie temperature, provided its P–V–T equation of state is known. In practice, we found that although some data are available (see *e.g.* Besson & Nicol, 1990; Zhang & Guyot, 1999*a*) they are insufficient to allow the P–V–T equation of state to be extended above 1073 K and so data above this temperature (marked with the symbol '‡' in Table 2) were not used in fitting the (MgFe)O equations of state [the effect of pressure on this transition temperature is negligible (Leger *et al.*, 1972)].

Having determined the pressure at each state point measured, an exactly analogous procedure to that described above may then be used to determine the corresponding P–V–T equation-of-state parameters for the $Mg_{1-x}Fe_xO$ samples, by fitting this model to the data using nonlinear least-squares refinement. Initially, each composition was analysed separately, using the program *EOSFIT 5.2* (Angel, 2000) to determine V_o, K_{To}, $\partial K_T/\partial T$ and α. In view of the restricted pressure and temperature range of the measurements for each composition, K'_o was fixed at a value of 4 (corresponding to a second-order Birch–Murnaghan equation) and α was assumed to be constant throughout the temperature range. The estimated uncertainties in both P and V were used in the weighting scheme for the refinements.

On completing this analysis it became apparent that the results from the MgO sample showed a large systematic difference from those from the (Mg,Fe)O samples; in particular, the value of K_{To} for MgO that was obtained [195 (3) GPa] was 25 GPa higher than the mean value for the (Mg,Fe)O samples and about 30 GPa higher than the expected value for MgO (see below). We believe that the reason for this lies in the different way in which the pressure calibrant was introduced, which appears to have led to a systematic overestimate of the pressure applied to the MgO sample; for the MgO sample, a small piece of iron foil was placed at the centre of the sample volume, whereas for the (Mg,Fe)O sample, iron powder was mixed with the samples. The reason for this discrepancy is not clear, since it seems most unlikely that the temperature or pressure gradients within the sample could be sufficiently large to produce this effect (see *e.g.* Dobson, 2000; Klotz *et al.*, 2006). Whatever the reason, it was clear that the two experimental configurations were not equivalent and so it was decided that the MgO data should be excluded from the analysis.

We believe that the present study represents the first attempt to measure the Anderson–Grüneisen parameter of (Mg,Fe)O for a wide range of compositions in a single set of experiments. The weighted means of the three values of $\partial K_T/\partial T$ and of K_{To} that we obtained were $\sim$0.024 (13) GPa K^{-1} and 170 (4) GPa, in good agreement with those published previously (see above). However, the three values of $\partial K_T/\partial T$ for x = 0.4, 0.3 and 0.2 [−0.028 (33), −0.039 (20) and −0.007 (21) GPa K^{-1}, respectively] and of K_{To} [177 (16), 168 (5) and 172 (8) GPa] did not show a systematic trend with composition and in the case of $\partial K_T/\partial T$ their estimated standard uncertainties were of similar magnitude to the values themselves. It was apparent from this that our results were not sufficiently precise to allow determination of any variation of $\partial K_T/\partial T$ with composition and it was, therefore, decided to combine all 60 P–V–T points into a single data set, to be fitted simultaneously, assuming that the equation-of-state parameters either varied linearly, or were invariant, with composition, *i.e.* for material of composition $Mg_{1-x}Fe_xO$,

$$K_T(x, T) = K_T(\mathrm{MgO}, T_{\mathrm{ref}}) + (\partial K_T/\partial x)x + (\partial K_T/\partial T)(T - T_{\mathrm{ref}}) \quad (6)$$

and

$$\alpha(x) = \alpha(\mathrm{MgO}) + (\partial\alpha/\partial x)x, \quad (7)$$

with $(\partial K_T/\partial x)$, $(\partial K_T/\partial T)$ and $(\partial\alpha/\partial x)$ constant for all values of x. We believe that this approach is adequate for present purposes, although the results of Reichmann *et al.* (2000) suggest that, at least for the elastic constant c_{11}, simple interpolation between MgO and FeO may give erroneous results.

A general-purpose nonlinear least-squares Fortran program was modified to allow this model to be fitted. To eliminate the systematic volume offsets between the three loadings of the high-P/T cell, the volumes used in the fitting were first normalized by their appropriate values of V_o, as determined above. The model was fitted with respect to a reference temperature, T_{ref}, of 300 K and to further reduce the number of free parameters a value of α for MgO of 3.16×10^{-5} K^{-1} (Fei, 1995) was adopted; as before, the estimated uncertainties in both P and V/V_o were used in the weighting scheme for the refinements. The variable parameters for the refinement were,

Table 3
(*a*) Fitted thermoelastic parameters and (*b*) isothermal Anderson–Grüneisen parameter for $Mg_{1-x}Fe_xO$.

Extrapolated values are shown in italics. α(MgO) was not varied in the refinement. For details see text.

(*a*) Fitted thermoelastic parameters.

K_{To}(MgO, 300)	173 (7) GPa
$\partial K_{To}/\partial x$	−18 (23) GPa atom^{-1}
$\partial K_T/\partial T$	−0.024 (9) GPa K^{-1}
α(MgO)	3.16×10^{-5} K^{-1}
$\partial\alpha/\partial x$	1.3 (4) $\times 10^{-5}$ K^{-1} atom^{-1}

(*b*) Isothermal Anderson–Grüneisen parameter.

x	*0.0*	0.2	0.3	0.4	*1.0*
δ_T	*4.4 (17)*	4.1 (16)	4.0 (16)	3.9 (15)	*3.4 (15)*

therefore, K_{To}(MgO, 300), $\partial K_{To}/\partial x$, $\partial K_T/\partial T$ and $\partial\alpha/\partial x$. The values of the refined parameters are shown in Table 3(*a*), with the corresponding values of the isothermal Anderson–Grüneisen parameter for the different (MgFe)O compositions given in Table 3(*b*). In Table 3(*b*), the model is also extrapolated to show the expected values for the MgO and FeO end members (values displayed in italics); it should be noted, however, that the extrapolation to FeO should be treated with caution as the thermoelastic properties of Fe_xO are complicated by its defect concentration and defect structures (Zhang, 2000), which may be altered at elevated temperatures by the exsolution of magnetite (Zhang & Zhao, 2005).

It can be seen from Table 3 that the values for $\partial K_T/\partial T$ [−0.024 (9) GPa K^{-1}] and for δ_T [∼4.0 (16)] that we have obtained in the present work are in very good agreement with the computational and experimental results (Table 1) published previously; it should be noted that the value of $\partial K_T/\partial T$ in Table 3 is identical to that obtained above by fitting the data for each composition separately, though the precision is improved by the use of the combined data set. The values of δ_T vary slightly with composition, but it should be remembered that the method of analysis used restricts any such dependence only to that arising from the variation in α and K_T. In particular, our results agree well with the experiments of Fei *et al.* (1992) [$\partial K_T/\partial T = -0.027$ (3) GPa K^{-1}, $\delta_T = 4.3$ (5)], Zhang & Kostak (2002) [$\partial K_T/\partial T = -0.029$ (3) GPa K^{-1}, $\delta_T = 5.3$ (6)] and van Westrenen *et al.* (2005) [$\partial K_T/\partial T = -0.020$ (1) GPa K^{-1}, $\delta_T = 3.3$ (1)]. However, although accurate, our values are less precise than those produced by these three X-ray diffraction studies, probably because of the smaller pressure range available to us in our experiments and, relative to the work of van Westrenen *et al.* (2005), the much smaller data set used.

The agreement of the remaining parameters listed in Table 3 with previously published results is also good, although, in general, their values are not determined very precisely. The value for K_{To}(MgO, 300), 173 (7) GPa, is a little higher than those given by, for example, Sumino *et al.* (1983) (160.5 GPa), Isaak *et al.* (1989) [161.6 (6) GPa] and Fei (1999) [160 (2) GPa], but still lies within two standard uncertainties of these results; it is, however, also possible that our higher value of K_{To} may reflect a small systematic error in the pressure calibration resulting from our choice of the equation of state parameters for iron. The value of $(\partial K_{To}/\partial x)$ [−18 (23) GPa per atom of Fe in the chemical formula] leads to $K_{To} = 166$ (12) GPa for the composition $Mg_{0.6}Fe_{0.4}O$; again, this is in reasonable agreement with the values of Fei *et al.* (1992), Zhang & Kostak (2002) and van Westrenen *et al.* (2005), who found $K_{To} = 157$, 158 (2) and 155 (2) GPa, respectively. By continuing the linear extrapolation of our results, K_{To} is found to be equal to 155 (24) GPa for FeO; this is within the range of values for Fe_xO reported by Zhang (2000) and comparable to that [146 (2) GPa] reported by Jacobsen *et al.* (2005); Fei (1999) also found $K_{To} = 146$ GPa, for FeO, with $(\partial K_{To}/\partial x) = -14$ GPa atom^{-1}, the latter value being very similar to that obtained here. Finally, on the basis of the thermal expansion coefficients for MgO and FeO listed by Fei (1995), we would expect $(\partial\alpha/\partial x) = 0.23 \times 10^{-5}$ K^{-1} atom^{-1}. Our fitted value of this parameter, 1.3 (4) $\times 10^{-5}$ K^{-1} atom^{-1}, is, therefore, too large, although this may simply reflect the fact that it is poorly determined owing to the limited range of composition of the samples.

The experiments reported here required only about 3.5 days of beamtime at ISIS and thus time-of-flight neutron powder diffraction can now be considered to be a relatively rapid technique for determining *P–V–T* equations of state. The high-*P*/*T* cell as described by Le Godec *et al.* (2001), which is now available to users of ISIS as a standard sample environment, provides 'clean' diffraction patterns in the range $P <$ 6 GPa. It can, therefore, be regarded as a very suitable experimental setup for studying materials that are elastically fairly soft, for example those with K_T less than ∼60 GPa, for which $\eta = 0.92$ at 6 GPa. For the study of stiffer materials, however, such as those examined in the present work, where $K_T \simeq 160$ GPa, it will be necessary to extend the accessible pressure range to ∼15 GPa to obtain this compression ratio. At present, even with the toroidally gasketed cell, we have not yet been able to achieve this value, 12 GPa and 1200 K representing the upper limits of the current apparatus. We are hopeful, however, that, by employing the toroidal gaskets in combination with sintered diamond anvils, pressures and temperatures approaching 20 GPa and 2300 K may be attainable in the near future. If this can be done, neutron methods should then be able to produce results, even for fairly incompressible materials, of similar precision to those currently obtained by X-ray diffraction. Neutron diffraction would then have some advantages over energy-dispersive X-ray methods using multi-anvil presses in giving better resolution and producing data that are more suitable for structure refinement purposes. Similarly, the method would have advantages over X-ray diffraction with externally heated diamond-anvil cells in that it should be possible to achieve stable temperatures that are far higher, with the further advantage that the sample temperature may be measured by neutron absorption resonance radiography. Unlike thermocouples, this method is not subject to failure during the experiment, nor is it dependent upon largely unknown, or at

best poorly determined, pressure coefficients of thermocouple electro-motive forces. Recent developments in the resonance radiography method (Stone *et al.*, 2006) indicate that, by the use of Hf rather than Ta foils, a precision of ± 10 K is achievable, which is generally adequate for equation-of-state studies.

LV and DPD gratefully acknowledge receipt of Royal Society University Research Fellowships; DD also wishes to acknowledge funding from the EU 'Research Infrastructures: Trans-national Access' Programme [contract No. 505320 (RITA) – High Pressure] awarded to the Bayerisches Geoinstitut. ADF acknowledges funding from the Science and Technology Facilities Council (ref. PPA/P/S/2003/00247). The authors are grateful to the ISIS facility for beam time to carry out this experiment and to the ISIS support staff for technical assistance.

References

Aizawa, Y. & Yoneda, A. (2006). *Phys. Earth Planet. Inter.* **155**, 87–95.

Anderson, O. L. & Isaak, D. G. (1993). *J. Phys. Chem. Solids*, **54**, 221–227.

Anderson, O. L. & Isaak, D. G. (2000). *Am. Mineral.* **85**, 376–385.

Angel, R. J. (2000). *High-Pressure, High-Temperature Crystal Chemistry*, Reviews in Mineralogy and Geochemistry, Vol. 41, edited by R. M. Hazen & R. T. Downs, pp. 35–60. Washington, DC: Mineralogical Society of America/The Geochemical Society.

Angel, R. J., Ross, N. L., Wood, I. G. & Woods, P. A. (1992). *Phase Transitions*, **39**, 13–32.

Badro, J., Fiquet, G., Guyot, F., Rueff, J-P., Struzhkin, V. V., Vankó, G. & Monaco, G. (2003). *Science*, **300**, 789–791.

Bailey, I. F. (2003). *Z. Kristallogr.* **218**, 84–95.

Bina, C. R. & Helffrich, G. R. (1992). *Annu. Rev. Earth Planet. Sci.* **20**, 527–552.

Besson, J. M. & Nicol, M. (1990). *J. Geophys. Res.* **95**, 21717–21720.

Chopelas, A. (1990). *Phys. Chem. Miner.* **17**, 142–148.

Deschamps, F., Trampert, J. & Tackley, P. J. (2005). *Geochim. Cosmochim. Acta*, **69** (Suppl.), A431.

Dewaele, A., Fiquet, G., Andrault, D. & Hausermann, D. (2000). *J. Geophys. Res.* **105**, 2869–2877.

Dobson, D. P. (2000). *Phys. Earth Planet. Inter.* **120**, 137–144.

Dong, Y.-H., Liu, J., Li, Y.-C. & Li, X.-D. (2003). *J. Appl. Cryst.* **36**, 1123–1127.

Duffy, T. S., Hemley, R. J. & Mao, H. K. (1995). *Phys. Rev. Lett.* **74**, 1371–1374.

Fei, Y. (1995). *Thermal Expansion*, in *Mineral Physics and Crystallography, A Handbook of Physical Constants*, edited by T. J. Ahrens. Washington, DC: AGU.

Fei, Y. (1999). *Am. Mineral.* **84**, 272–276.

Fei, Y., Mao, H.-K., Shu, J. & Hu, J. (1992). *Phys. Chem. Mineral.* **18**, 416–422.

Fei, Y. & Wang, Y. (2000). *High-Pressure, High-Temperature Crystal Chemistry*, Reviews in Mineralogy and Geochemistry, Vol. 41, edited by R. M. Hazen & R. T. Downs, pp. 521–557. Washington, DC: Mineralogical Society of America/The Geochemical Society.

Fortes, A. D., Wood, I. G., Alfredsson, M., Vočadlo, L. & Knight, K. S. (2006). *Eur. J. Mineral.* **18**, 449–462.

Gillan, M. J., Alfè, D., Brodholt, J., Vočadlo, L. & Price, G. D. (2006). *Rep. Prog. Phys.* **69**, 2365–2441.

Guignot, N., Andrault, D., Morard, G., Bolfan-Casanova, N. & Mezouar, M. (2007). *Earth Planet. Sci. Lett.* **256**, 162–168.

Hama, J. & Suito, K. (1999). *Phys. Earth Planet. Inter.* **114**, 165–179.

Inbar, I. & Cohen, R. E. (1995). *Geophys. Res. Lett.* **22**, 1533–1536.

Isaak, D. G. (1990). *J. Geophys. Res.* **95**, 7055–7067.

Isaak, D. G., Anderson, O. L. & Goto, T. (1989). *Phys. Chem. Miner.* **16**, 704–713.

Isaak, D. G. & Masuda, K. (1995). *J. Geophys. Res.* **100**, 17689–17698.

ISIS Annual Report (1996). Report RAL-TR-96-050, pp. 61–62. Rutherford Appleton Laboratory, Didcot, Oxfordshire, UK.

Jackson, J. M., Sinogeikin, S. V., Jacobsen, S. D., Reichmann, H. J., Mackwell, S. J. & Bass, J. D. (2006). *J. Geophys. Res.* **111**, B09203.

Jacobsen, S. D., Lin, J.-F., Angel, R. J., Shen, G., Prakapenka, V. B., Dera, P., Mao, H.-k. & Hemley, R. J. (2005). *J. Synchrotron Rad.* **12**, 577–583.

Jacobsen, S. D., Reichmann, H.-J., Spetzler, H. A., Mackwell, S. J., Smyth, J. R., Angel, R. J. & McCammon, C. A. (2002). *J. Geophys. Res.* **107**(B2), 2037.

Jacobsen, S. D., Spetzler, H. A., Reichmann, H-J. & Smyth, J. R. (2004). *Proc. Natl Acad. Sci. USA*, **101**, 5867–5871.

Jacobsen, S. D., Spetzler, H. A., Reichmann, H.-J., Smyth, J. R., Mackwell, S. J., Angel, R. J. & Bassett, W. A. (2002). *J. Phys. Condens. Matter*, **14**, 11525–11530.

Kantor, I., Dubrovinsky, L., McCammon, C., Kantor, A., Pascarelli, S., Aquilanti, G., Crichton, W., Mattesini, M., Ahuja, R., Almeida, J. & Urusov, V. (2006). *Phys. Chem. Miner.* **33**, 35–44.

Khvostantsev, L. G., Sidorov, V. A. & Tsiosk, O. B. (1998). *High Pressure Toroid Cell: Applications in Planetary and Material Sciences*, in *Properties of Earth and Planetary Materials at High Pressure and Temperature*, edited by M. H. Manghnani & T. Yagi. Washington, DC: AGU.

Khvostantsev, L. G., Slesarev, V. N. & Brazhkin, V. V. (2004). *High Pressure Res.* **24**, 371–383.

Khvostantsev, L. G., Vereshchagin, L. F. & Nivikov, A. P. (1977). *High Temp. High Pressures*, **9**, 637–639.

Klotz, S., Besson, J. M. & Hamel, G. (2006). *High Pressure Res.* **26**, 277–282.

Larson, A. C. & Von Dreele, R. B. (2000). *GSAS*, *General Structure Analysis System*. Report LAUR 86–748. Los Alamos National Laboratory, New Mexico, USA.

Leger, J. M., Loriers-Susse, C. & Vodar, B. (1972). *Phys. Rev. B*, **6**, 4250–4261.

Le Godec, Y., Dove, M. T., Francis, D. J., Kohn, S. C., Marshall, W. G., Pawley, A. R., Price, G. D., Redfern, S. A. T., Rhodes, N., Ross, N. L., Schofield, P. F., Schooneveld, E., Syfosse, G., Tucker, M. G. & Welch, M. D. (2001). *Mineral. Mag.* **65**, 737–748.

Lin, J.-F., Struzhkin, V. V., Jacobsen, S. D., Hu, M. Y., Chow, M. Y., Kung, J., Liu, H., Mao, H.-k. & Hemley, R. J. (2005). *Nature* (*London*), **436**, 377–380.

Matsui, M. (1989). *J. Chem. Phys.* **91**, 489–494.

Matsui, M., Parker, S. C. & Leslie, M. (2000). *Am. Mineral.* **85**, 312–316.

Mattern, E., Matas, J., Ricard, Y. & Bass, J. (2005). *Geophys. J. Int.* **160**, 973–990.

Miletich, R., Allan, D. R. & Kuhs, W. F. (2000). *High-Pressure, High-Temperature Crystal Chemistry*, Reviews in Mineralogy and Geochemistry, Vol. 41, edited by R. M. Hazen & R. T. Downs, pp. 445–519. Washington, DC: Mineralogical Society of America/The Geochemical Society.

Murakami, M., Hirose, K., Kawamura, K., Sata, N. & Ohishi, Y. (2004). *Science*, **304**, 855–858.

Oganov, E. R. & Ono, S. (2004). *Nature* (*London*), **430**, 445–448.

Poirier, J.-P. (2000). *Introduction to the Physics of the Earth's Interior*, 2nd ed. Cambridge University Press.

Reichmann, H.-J., Jacobsen, S. D., Mackwell, S. J. & McCammon, C. A. (2000). *Geophys. Res. Lett.* **27**, 799–802.

Reynard, B. & Price, G. D. (1990). *Geophys. Res. Lett.* **17**, 689–692.

Richet, P., Mao, H.-K. & Bell, P. M. (1989). *J. Geophys. Res.* **94**, 3037–3045.

Ringwood, A. E. (1962). *J. Geophys. Res.* **67**, 4005–4010.

Rosenhauer, M., Mao, H.-K. & Woermann, E. (1976). *Year Book*, Vol. 75, pp. 513–515. Carnegie Institution of Washington.

Rotter, C. A. & Smith, C. S. (1966). *J. Phys. Chem. Solids*, **27**, 267–276.
Samuel, H., Farnetani, C. G. & Andrault, D. (2005). *Heterogeneous Lowermost Mantle: Compositional Constraints and Seismological Observables*, in *Earth's Deep Mantle: Structure, Composition, and Evolution*, edited by R. D. van der Hilst, J. Bass, J. Matas & J. Trampert, pp. 103–118. Washington, DC: AGU.
Scott, H. P., Williams, Q. & Knittle, E. (2001). *Geophys. Res. Lett.* **28**, 1875–1888.
Shim, S.-H., Catalli, K., Hustoft, J., Kubo, A., Prokapenka, V. B., Caldwell, W. A. & Kunz, M. (2008). *Proc. Natl Acad. Sci. USA*, **105**, 7382–7386.
Shim, S-H., Duffy, T. S. & Shen, G. (2001). *Science*, **293**, 2437–2440.
Smith, D. K. & Newkirk, W. (1965). *Acta Cryst.* **18**, 983–991.
Speziale, S., Zha, C.-S., Duffy, T. S., Hemley, R. J. & Mao, H.-k. (2001). *J. Geophys. Res.* **106**, 515–528.
Stone, H. J., Tucker, M. G., Le Godec, Y., Méducin, F. M., Cope, E. R., Hayward, S. A., Ferlat, G. P. J., Marshall, W. G., Manolopoulos, S., Redfern, S. A. T. & Dove, M. T. (2005). *Nucl. Instrum. Methods Phys. Res. Sect. A*, **547**, 601–615.
Stone, H. J., Tucker, M. G., Méducin, F. M., Dove, M. T., Redfern, S. A. T., Le Godec, Y. & Marshall, W. G. (2006). *J. Appl. Phys.* **98**, 064905.
Sumino, Y., Anderson, O. L. & Suzuki, I. (1983). *Phys. Chem. Miner.* **9**, 38–47.
Toby, B. H. (2001). *J. Appl. Cryst.* **34**, 210–213.
Trampert, J., Deschamps, F., Resovsky, J. & Yuen, D. (2004). *Science*, **306**, 853–856.
Utsumi, W., Weidner, D. J. & Liebermann, R. C. (1998). *Properties of Earth and Planetary Materials at High Pressure and Temperature*, edited by Y. SyoNo & M. H. Manghnani, pp. 327–333. Washington, DC: AGU.
Vočadlo, L. (2007). *Earth Planet. Sci. Lett.* **254**, 227–232.
Vočadlo, L., Alfè, D., Gillan, M. J. & Price, G. D. (2003). *Phys. Earth. Planet. Inter.* **140**, 101–125.
Westrenen, W. van, Li, J., Fei, Y., Frank, M. R., Hellwig, H., Komabyashi, T., Mibe, K., Minarik, W. G., Van Orman, J. A., Watson, H., Funakoshi, K. & Schmidt, M. W. (2005). *Phys. Earth. Planet. Inter.* **151**, 163–176.
Zhang, J. (2000). *Phys. Rev. Lett.* **84**, 507–510.
Zhang, J. & Guyot, F. (1999*a*). *Phys. Chem. Miner.* **26**, 206–211.
Zhang, J. & Guyot, F. (1999*b*). *Phys. Chem. Miner.* **26**, 419–424.
Zhang, J. & Kostak, P. (2002). *Phys. Earth Planet. Int.* **129**, 301–311.
Zhang, J. & Zhao, Y. (2005). *Phys. Chem. Miner.* **32**, 241–247.
Zhang, L. & Gong, Z.-Z. (2006). *Chin. Phys. Lett.* **23**, 3049–3051.
Zhao, Y., Von Dreele, R. B. & Morgan, J. G. (1999). *High Pressure Res.* **16**, 161–177.